Molecular dynamics of irradiation-induced defect production in GaN nanowires

Wei Ren,[*] Antti Kuronen, and Kai Nordlund

Department of Physics, University of Helsinki, P.O. Box 64, FIN-00014 Helsinki, Finland
(Received 9 March 2012; revised manuscript received 4 September 2012; published 27 September 2012)

We have used classical molecular dynamics methods to simulate the defect production of small-cross-section GaN nanowires by Ar ion irradiation. We performed 200 random individual ion impacts in the energy range of 30 eV to 10 keV for each nanowire. We found that the defect production for all nanowires was greatly enhanced in the low ion energy range below 3 keV, while at higher energies the defect production decreased due to the increasing transmission of ions through small-cross-section nanowires. Owing to the strong surface enhancement of defect production, in the low-energy range, the defect production in the nanowires was increased by a factor of 2 compared to bulk GaN. A simple model to estimate the irradiation energy dependence of the damage production in a nanowire was developed. It is based on the Gaussian energy deposition profile, and it gives the irradiation energy of the maximum damage in a reasonable agreement with the simulation results.

I. INTRODUCTION

Semiconductor nanowires (NWs) are considered to be of great importance for future nanotechnology applications.[1] Due to the roles of dimensionality and small system size, NWs have great potential for testing and understanding fundamental concepts, such as optical, electrical, and mechanical properties.[2,3] Potential industrial applications of nanowires range from field-effect transistors[4,5] to biological applications.[6,7] GaN is a compound semiconducting material attracting great interest because its band gap is relatively large, which has a significant application in optoelectronic nanodevices.[8]

Recent experiments show that irradiation of nanomaterials with energetic ions or electrons induces atomic defect production[9] in the target. This effect can be used to modify the mechanical and electronic properties of the nanomaterials. It is not obvious whether irradiation of a nanowire enhances or reduces the damage compared to bulk. Thus, a fundamental understanding of defect formation under irradiation and how defects affect the material properties is of great interest. In this paper, classical molecular dynamics (MD) simulation was used to examine the irradiation-induced defect-formation process in small-diameter hexagonal GaN NWs. The density distribution of the defects was analyzed to examine the importance of surface enhancement of defect production. We further compared the defect production in GaN NWs with that in bulk GaN, which was irradiated by self-recoiling atoms, and also with defect production in Si NWs under the same Ar irradiation conditions. We found that nanoscale effects in the nanowires made it different from bulk GaN in defect production. Finally, we determined how the defects modified the mechanical properties of NWs by obtaining Young's modulus of both perfect and defective GaN NWs.

II. SIMULATION METHOD

The irradiation processes were simulated by using the classical MD method with the PARCAS code.[10] The cells of GaN NWs were created in the wurtzite crystal structure. Two different diameter sizes of NWs were used. The smaller NW had an ∼3 nm diameter with 7052 atoms, and the larger one had an ∼4 nm diameter with 12 925 atoms. Both of the NWs had lengths of ∼10 nm. The systems were relaxed from a temperature of 600 to 0 K slowly for 80 ps using the Berendsen pressure control.[11] After relaxation, both NWs had two different reconstructions on the facets and two different reconstructions on the edges. The relaxed systems are illustrated in Fig. 1.

For modeling the Ga-N, Ga-Ga, and N-N interactions, the analytic bond-order potential[12] of the Tersoff-Brenner[13] form was used. This potential did not include long-range Coulombic interactions, but it provided a good fit to many properties[12] of different GaN structures, such as elastic moduli, melting point, and solubility.[12] One should also note that the inclusion of explicit ionic charges (so-called dynamic charge-transfer model) has been tested to have only minor effects on the defect production in irradiation simulations.[14,15] For modeling Ar-Ga and Ar-N interactions, a purely repulsive ZBL potential[16] was used because of the dominating screened Coulombic interactions in high-energy collisions. Additionally, a repulsive ZBL pair potential was used to describe Ga-N, Ga-Ga, and N-N interactions in the high-energy part.

Periodic boundary conditions along the longitudinal axis of the NWs were used to mimic wires with infinite length. Since both NWs had two different facet and edge reconstructions, irradiation has been performed on both two facets and two edges for each NW. The recoiling Ar atom bombarded the NWs perpendicularly on the facets and edges. For each set of irradiations, 200 individual uniformly random points were chosen on two-dimensional facets and one-dimensionally along the edges. The sets of irradiation always started from the relaxed systems. To make sure each energetic ion bombarded the central point of the system, the NW was shifted along its longitudinal axis after each random point was chosen because of the boundary conditions along the length of NWs. Each impact was simulated for 50 ps. Ar ion energies of 30, 100, 300, 1000, 3000, and 10 000 eV were used for each set of simulations. Berendsen temperature control[11] was used near the periodic boundaries to dissipate heat from the impact region into other parts of the NW, and all the simulations were performed at a temperature of 0 K.

After the irradiation simulations, the defects in the last configuration of the systems were analyzed by the Voronoy-
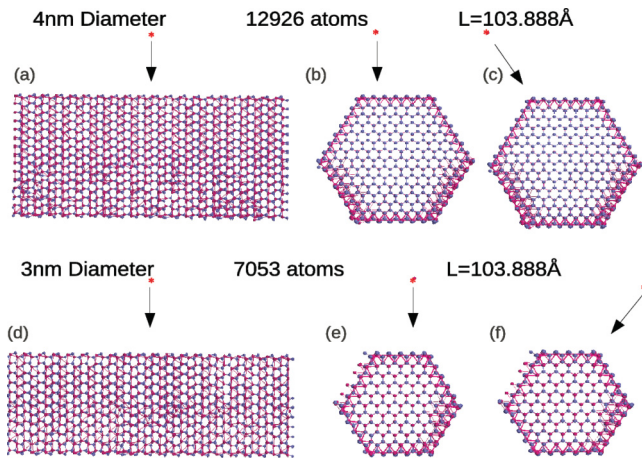
FIG. 1. (Color online) Visualizations of the relaxed NWs. (a) Side view of the 4-nm-diameter NW. (b) Cross section of the 4-nm-diameter NW with an incident ion on the flat surface. (c) Cross section of the 4-nm-diameter NW with an incident ion on the edge. (d) Side view of the 3-nm-diameter NW. (e) Cross section of the 3-nm-diameter NW with an incident ion on the flat surface. (f) Cross section of the 3-nm-diameter NW with an incident ion on the edge. The NWs of both diameters had two different facets and edges, which were facet 1, facet 2, edge 1, and edge 2.

polyhedron approach.[17] Vacancies and interstitials can be found using this method. Additionally, any atom at the distance range of 1 to 3 Å from the NW surfaces was considered as an adatom, and any atom at a distance farther than 3 Å from the surfaces was considered as sputtered.

III. RESULTS

To illustrate the defect production process during irradiation, five snapshots of a 3-keV Ar impact on surface facet 1 of the 4-nm GaN NW are presented in Fig. 2. Initially, the recoiling Ar atom has not hit the surface, and the structure of the wire is a perfect crystal without any atoms displaced from the lattice sites. At 0.05 ps, the Ar atom has penetrated a 1–2 nm distance from the surface into the wire, but the small collision cascades are mainly focused near the surface. At 0.15 ps, the Ar atom has penetrated half of the cross section of the wire, inducing many displacements in the top half of the wire. At 0.775 ps, the collision cascade has spread through the entire cross section of the wire. At 40 ps, the damaged regions decrease in size due to defect annealing.

Results of defect production for Ar irradiation on surface facets of each NW and for self-recoil atoms in bulk GaN are presented as a function of the ion energy in Fig. 3. Data for the self-recoil irradiation in bulk GaN were obtained from Ref. 18. With the ion energy increasing, the defect production in bulk GaN increases nearly linearly. In the low-energy region the defect production for Ga irradiation on bulk GaN shows a little larger values compared with N irradiation on bulk GaN, while in the high ion energy region they behave in the opposite way. However, the defect production in NWs is clearly different. With the ion energy increasing, the defect production reaches a maximum value at 3 keV for both 3- and 4-nm-diameter NWs and for all facets, approximately a factor of 2 more compared to the values of bulk GaN. The defect
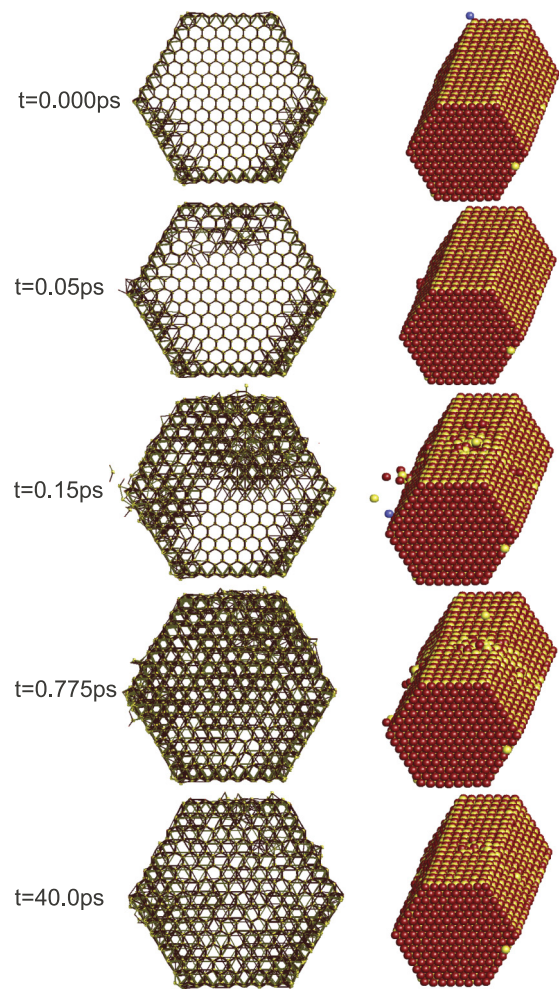
FIG. 2. (Color online) Snapshots of a 3-keV Ar impact on facet 1 of the 4-nm NW. (left) The cross sections of the NW at different time scales, plotting atoms and covalent bonds. (right) The same NW in a three-dimensional view at the same time steps, with atoms colored by type.

production of the 3-nm-diameter NWs shows more significant enhancements compared to the 4-nm-diameter NWs for both facets 1 and 2 owing to the greater surface-to-volume ratio. In the high ion energy region, the defect production for each NW decreases. This is because at high irradiation energies the transmission of ions increases, inducing fewer collisions in the NWs. Hence, the defect production of self-recoils on bulk GaN shows significantly larger values than both NWs at the higher irradiation energies.

The surface-to-volume ratio effect of defect production can be understood by the fact that the defects are predominantly created on the surfaces of the NWs, which is common for nanomaterials. Figure 4 shows the radial density distribution of defect production as measured from the center of both NWs created at the 3-keV irradiation energy. It is shown that the defect production for both NWs is concentrated at distances ~15 and ~20 Å from the center, which are the positions of the atomic outermost layers of both NWs. The fact that the defect density is larger for the 3-nm NW can be attributed to the larger surface-to-volume ratio of the 3-nm NW compared to that of the 4-nm NW. After the irradiation simulations, the
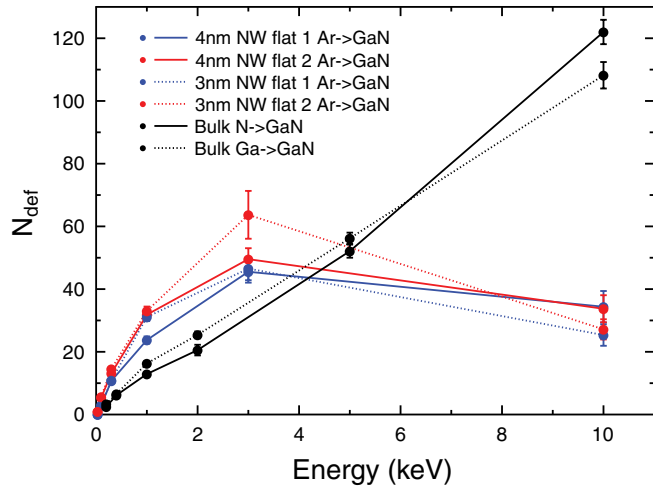
FIG. 3. (Color online) The results of defect production for self-recoil irradiation on bulk GaN and Ar ion irradiation on 3-nm and 4-nm diameter NWs for facets 1 and 2.

FIG. 5. (Color online) The results for four different types of defects, vacancies, interstitials, adatoms, and sputtered atoms, for the 3-nm-diameter NW, facet 2.

wires remained almost intact except for some damaged regions at the surfaces.

The contributions to the total defect production from different defect types are presented in Fig. 5. It can be seen that with increasing ion energy, the defects of four different types have the same tendencies as the total defect production, reaching the maximum value at 3-keV energy. Adatoms show the least contribution, with a very small number, less than 4, while sputtered atoms show the second smallest contribution to the total defect production. Vacancies are predominant, contributing half of the total number of defects. This is obviously due to atom number conservation.[19]

The results of defect productions for both the 3- and 4-nm-diameter NWs and for different facets and edges are

presented in Fig. 6. It is shown that whether the ion impinges on a surface or on an edge makes a great difference in defect production. Ion irradiation on facets generally shows more significant enhancements than irradiation on edges. In general, when the incident ions are irradiated through the wires, the channeling effects on the edges are stronger than on the surfaces, and consequently, the stopping power is smaller. This can be easily seen by investigating the wurtzite structure
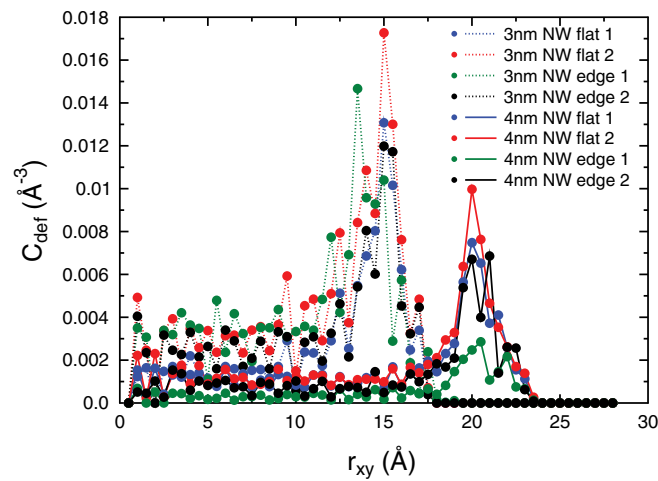
FIG. 4. (Color online) Radial density of the defects as measured perpendicularly from the NW axis. Density of vacancies and interstitials for both 3- and 4-nm-diameter NWs for facet 1, facet 2, edge 1, and edge 2, created by a 3-keV Ar ion are shown. The smallest distance from the surface to the center for the 3-nm-diameter NW is 15 Å, and the smallest distance for the 4-nm-diameter NW is 20 Å.
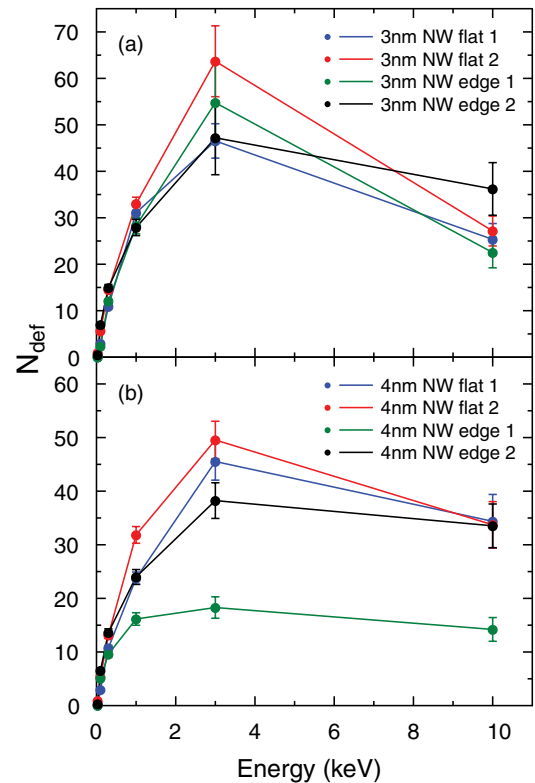
FIG. 6. (Color online) Total number of defects for facet 1, facet 2, edge 1, and edge 2. (a) Defect number for the 3-nm-diameter NW. (b) Defect number for the 4-nm-diameter NW.
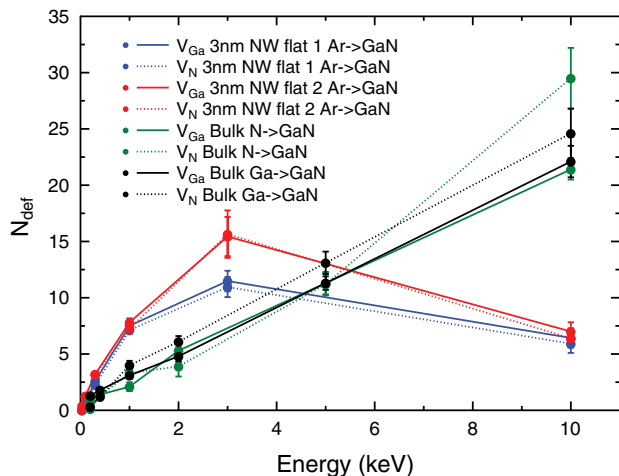
FIG. 7. (Color online) Results of vacancy numbers of Ga and N atoms for self-recoiling irradiation in bulk GaN and for Ar ion irradiation in 3-nm GaN NWs of facets 1 and 2, respectively.

from along the directions of the facets and edges used in the simulations. Additionally, Fig. 6 demonstrates again that the 3-nm wire has a stronger enhancement in defect production than the 4-nm wire because of the surface-to-volume ratio effect.

To understand the defect production of different atom types, the numbers of Ga and N vacancies were calculated since vacancies are predominant in defect production. A comparison of Ga and N vacancies is shown in Fig. 7 for smaller NWs with facet irradiation and for bulk GaN with self-recoil atom irradiation. With increasing irradiation energy, the tendencies of Ga and N vacancies for all the cases in Fig. 7 are consistent with the total defect production shown in Fig. 3. For bulk GaN, the numbers of both vacancy types are relatively close in the low ion energy range below 5 keV, while at high energy the number of N vacancies is slightly larger. However, for NWs, the numbers of vacancies of both Ga and N atoms do not show large differences, with similar values in the whole ion energy range.

The enhancement of irradiation-induced defect production in Si NWs was studied earlier by us.[19] A comparison of defect production of the 4-nm Si NW and GaN NW for different defect types is presented in Fig. 8(a). For both NWs, the vacancies show predominant contributions to total defect production, while adatoms contributed the least. The numbers of different defect types have the same dependence on the increasing ion energy for both GaN and Si NWs, with a defect production enhancement within the energy range 0–3 keV, and then decrease at higher energies for all the wires. Thus, we find that the irradiation-induced defect production in the 4-nm GaN NWs is quite similar to the defect production in the 4-nm Si NW. However, the relative difference of sputtered atoms between GaN and Si NWs is comparatively large in Fig. 8(a). The sputtered species are shown for GaN NWs in Fig. 8(b). It is apparent that the difference is due to a large number of sputtered N atoms. The number of sputtered Ga atoms is similar to the number of sputtered Si atoms. Note that nitrogen loss from the GaN surface has been observed in high-dose irradiation studies.[20,21]
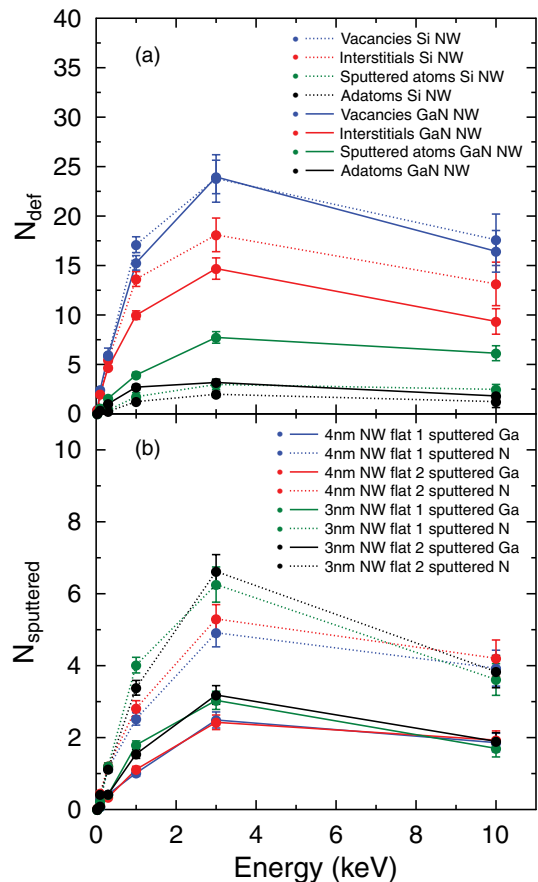
FIG. 8. (Color online) (a) Comparison of defect production of different types, vacancies, interstitials, adatoms, and sputtered atoms, between the 4-nm Si NW facet and 4-nm GaN NW facet 2. (b) Results of sputtered atoms numbers of Ga and N atoms for 3-nm GaN NWs and for 4-nm GaN NWs for facets 1 and 2, respectively.

The behavior of the damage production in nanowires, i.e., the amount of damage as a function of irradiation energy, can be explained by a simple mode that assumes that the damage distribution $F(x,y,z)$ produced in a *bulk* sample by an ion with energy E_{ion} has a double-Gaussian shape[22] [see Fig. 9(a)]:

$$F(x,y,z) = Ce^{-(y-y_0)^2/2\alpha^2}e^{-(x^2+z^2)/2\beta^2}, \quad (1)$$

where the normalization constant C is obtained from

$$\int_{-\infty}^{\infty} dx \int_{0}^{\infty} dy \int_{-\infty}^{\infty} dz \, F(x,y,z) = E_{\text{ion}} \quad (2)$$

as

$$C = \frac{E_{\text{ion}}}{\sqrt{2\pi^3}\alpha\beta^2[\text{erf}(y_0/\sqrt{2}\alpha) + 1]}. \quad (3)$$

The amount of damage in the nanowire is obtained by integrating the bulk damage density over the nanowire volume (see Fig. 9):

$$N_{\text{NW}} = 2\pi\beta^2 C \int_{0}^{2R} \text{erf}\left[\sqrt{\frac{y(2R-y)}{2\beta^2}}\right] e^{-(y-y_0)^2/2\alpha^2} dy. \quad (4)$$

Damage densities were obtained by fitting a three-dimensional Gaussian of Eq. (1) to vacancy depth profiles from binary collision approximation (BCA, SRIM[23]) calculations.
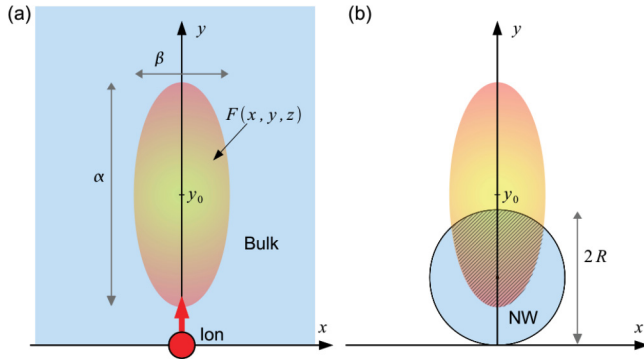
FIG. 9. (Color online) Arrangement used in the analytical model. (a) Damage distribution $F(x,y,z)$ centered at $(0,y_0,0)$ with widths α and β is obtained by simulating ions impinging on a bulk sample. (b) The amount of damage in a cylindrical nanowire located above the (x,z) plane with the central axis at $x=0, y=R$ is calculated by integrating the damage distribution calculated in (a) over the nanowire volume (hatched region).

By using only depth profiles the assumption of spherically symmetric damage density ($\alpha = \beta$) was made. The SRIM results along with the fitted Gaussian functions are shown in Fig. 10.

Figure 11 shows the comparison of the amount of damage in the nanowire calculated with the analytical model [Eq. (4)] and MD simulations. The qualitative behavior of the results of the analytical model is similar to the MD simulation: the maximum amount of damage is produced at irradiation energies around 3 keV. However, the absolute amount of damage cannot be estimated reliably from the results based on SRIM calculations because they do not include the damage annealing or the effect of the open surface to damage production threshold energies. Therefore, the curves for the analytical model in Fig. 11 are scaled to have the same area as the ones obtained from MD simulations. Nevertheless, the model could be used to determine the suitable energy range for ion irradiation of nanowires.

The sensitivity of the results of the model on the parameter values was investigated by varying the values of y_0 and α by
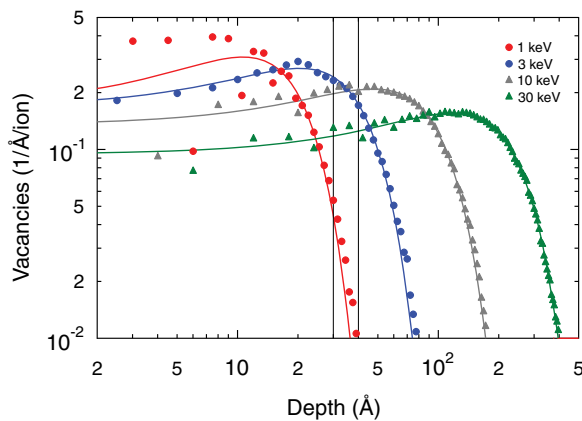
FIG. 10. (Color online) Depth profiles of vacancies as obtained from SRIM simulations (symbols) and corresponding fitted Gaussian functions (lines). The two vertical lines show the diameters of the NWs (3 and 4 nm) simulated in this work.
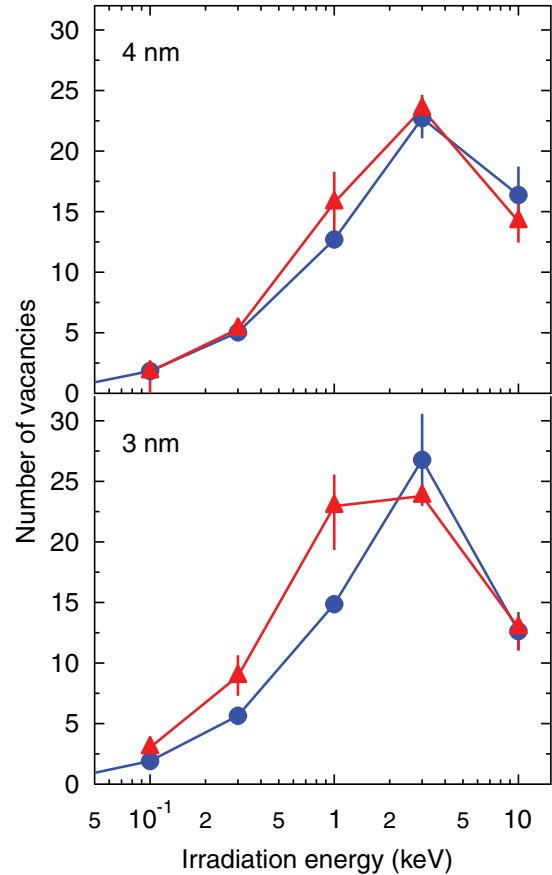
FIG. 11. (Color online) Comparison of the number of vacancies predicted by the analytical model (triangles) and MD simulations (circles). The areas of the curves of the analytical model are scaled to be the same as those of the MD simulation data. Error bars of the analytical curves describe the change in the results when the model parameters y_0 and α were varied by $\pm20\%$.

$\pm20\%$. The effect of this is shown as the error bars of the analytical model curves in Fig. 11. We can conclude that the result, i.e., the position of the maximum defect production, is not drastically affected by the variation.

To understand how defects influence mechanical properties of GaN NWs, Young's modulus along the axial direction was calculated from the results of elastic deformations, using atomistic simulations by LAMMPS.[24] Elastic stretching and compression simulations were done for both the perfect and defective NWs. For the case of stretching or compressing the wire, the elastic potential energy was calculated with the integral of this expression:

$$E = \int \frac{YA\triangle L}{L_0}\, d(\triangle L) = \frac{YA}{L_0}\int \triangle L\, d(\triangle L) = \frac{1}{2}YAL_0\varepsilon^2,$$

(5)

where A is the cross section of the wire, L_0 is the equilibrium length, and ε is the strain.

A parabola was fitted to the potential energy as a function of wire length:

$$E = aL^2 + bL + c.$$

(6)
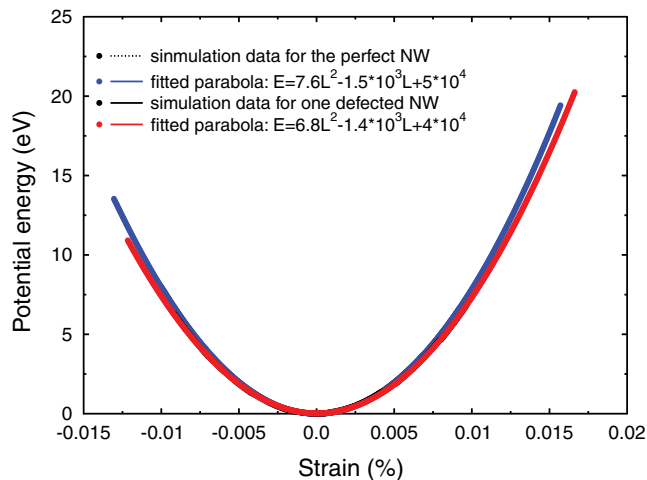
FIG. 12. (Color online) Strain dependence of the potential energy of the perfect and defective 3-nm NWs. The defective NW had 162 defects in total: 80 vacancies, 47 interstitials, 11 adatoms, and 24 sputtered atoms.

Young's modulus Y was then obtained by parameter b in the form (see the Appendix)

$$Y = -\frac{b}{A}. \qquad (7)$$

The simulation results of the potential-energy dependence on the wire lengths for both perfect and defective NWs are presented in Fig. 12. Calculations were performed for the perfect wire and ten defective 3-nm wires. Young's modulus for a perfect wire was obtained as 328 GPa and for the defective wires as 315 ± 5 GPa. Compared to Young's modulus of bulk GaN, which is 324 GPa in the [0001] direction,[25] the perfect wire's was quite near to this bulk value, while defects caused a small decrease in the Young's modulus value. Note that although the change is small, it was obtained by single ion impacts, at a fluence of about $(1 \text{ ion})/(30 \text{ nm}^2) \approx 3 \times 10^{12}$ ions/cm^2. Higher fluences could lead to larger softenings of the nanowire.

IV. DISCUSSION AND CONCLUSIONS

We have studied the defect production in GaN NWs under Ar ion irradiation using classical molecular dynamics simulations. The effect of the nanoscale dimensions of the irradiated object has a twofold effect on the damage production. At low energies damage production is enhanced when compared with a bulk target. With high enough energies less damage is produced in the nanowire than in the bulk.

The enhancement can be explained with surface effects. It was found that most of the defect production is concentrated near the surface of the NW. The formation energy of defects on and near the surface is known to be lower than in the bulk.[26] When the irradiation energy is so low that most of the energy of the ion is deposited to the NW, the strong surface enhancement causes the defect production of GaN NWs to become greater than bulk GaN. The defect production in the smaller-cross-section GaN nanowire shows a greater enhancement than the larger one because of the larger surface-to-volume ratio of the smaller nanowires.

When the irradiation energy is increased, the range of the ion and the extent of its energy deposition profile become comparable to the NW diameter. Increasing the energy further decreases damage production because more and more ions go through the NW, leaving less energy for damage production. Thus, there is an energy where the damage production is at its maximum. For Ar ions impinging on 3- and 4-nm GaN NWs this happens around 3 keV. For larger NWs this energy is expected to be larger.

The analytical model of damage production in the nanowires predicts the energy dependence of the damage, in reasonable agreement with the MD simulations results. One should note that the absolute value of the produced damage cannot be reliably predicted by BCA simulations because no defect annealing is included. However, the model could be used as a tool to estimate the optimal ion energy in nanowire irradiation experiments using fast BCA calculations instead of time-consuming MD simulations.

Compared to a Si NW under the same irradiation, the defect production of both GaN and Si materials was quite similar, and in both of them a strong surface enhancement was observed. There was, however, a pronounced difference in the amount of sputtering. This is explained by the large number of sputtered N atoms in the case GaN. Finally, defects in the GaN NW caused a small decrease in the Young's modulus of the wire. In summary, our simulations show that the defect productions in semiconductor NWs is strongly affected by small dimension and can be larger or smaller than that in the bulk targets.

APPENDIX: CALCULATION OF YOUNG'S MODULUS

Young's modulus Y is obtained from potential energy as a function of strain ε,

$$E(\varepsilon) = a'\varepsilon^2 + b'\varepsilon + c', \qquad (A1)$$

as

$$Y = \frac{2a'}{AL_0}, \qquad (A2)$$

where A is the cross section of the nanowire and L_0 is the equilibrium length. From simulations, the potential energy as a function of nanowire length L is obtained as

$$E(L) = aL^2 + bL + c, \qquad (A3)$$

where

$$L = (1 + \varepsilon)L_0. \qquad (A4)$$

Combing Eqs. (A3) and (A4), the coefficients of Eq. (A1) are expressed in terms of the coefficients of Eq. (A3) as

$$a' = aL_0^2, \quad b' = 2aL_0^2 + bL_0,$$
$$c' = aL_0^2 + bL_0 + c. \qquad (A5)$$

The equilibrium length L_0 is obtained as

$$\frac{dE(L)}{dL}\bigg|_{L=L_0} = 0, L_0 = -\frac{b}{2a}. \tag{A6}$$

Finally, using Eqs. (A5) and (A6), we get Young's modulus in terms of the coefficients of Eq. (A3):

$$Y = \frac{2a'}{AL_0} = \frac{2}{AL_0}aL_0^2 = \frac{2a}{A}\left(-\frac{b}{2a}\right) = -\frac{b}{A}. \tag{A7}$$

---

[*]wei.ren@helsinki.fi

[1]W. Lu and C. M. Lieber, J. Phys. D **39**, R387 (2006).

[2]A. P. Alivisatos, Science **271**, 933 (1996).

[3]A. M. Morales and C. M. Lieber, Science **279**, 208 (1998).

[4]Y. Cui, Z. Zhong, D. Wang, W. U. Wang, and C. M. Lieber, Nano Lett. **3**, 149 (2003).

[5]J. Goldberger, A. I. Hochbaum, R. Fan, and P. Yang, Nano Lett. **6**, 973 (2006).

[6]Y. Cui, Q. Wei, H. Park, and C. M. Lieber, Science **293**, 1289 (2001).

[7]G. Zheng, F. Patolsky, Y. Cui, W. U. Wang, and C. M. Lieber, Nat. Biotechnol. **23**, 1294 (2005).

[8]S. Nakamura, T. Mukai, and M. Senoh, J. Appl. Phys. **74**, 3911 (2009).

[9]A. V. Krasheninnikov and K. Nordlund, J. Appl. Phys. **107**, 071301 (2010).

[10]K. Nordlund, PARCAS computer code, 2006. The main principles of the molecular dynamics algorithms are presented in Refs. 27 and 28. The adaptive time step and electronic stopping algorithms are the same as in Ref. 29.

[11]H. J. C. Berendsen, J. P. M. Postma, W. F. van Gunsteren, A. DiNola, and J. R. Haak, J. Chem. Phys. **81**, 3684 (1984).

[12]J. Nord, K. Albe, P. Erhart, and K. Nordlund, J. Phys. Condens. Matter **15**, 5649 (2003).

[13]D. W. Brenner, Phys. Rev. Lett. **63**, 1022 (1989).

[14]J. W. Nord, Ph.D. thesis, University of Helsinki, 2003.

[15]K. Albe, J. Nord, and K. Nordlund, Philos. Mag. **89**, 3477 (2009).

[16]J. F. Ziegler, J. P. Biersack, and U. Littmark, *The Stopping and Range of Ions in Solids* (Pergamon, New York, 1985).

[17]K. Nordlund, M. Ghaly, R. S. Averback, M. Caturla, T. Diaz de la Rubia, and J. Tarus, Phys. Rev. B **57**, 7556 (1998).

[18]J. Nord, K. Nordlund, and J. Keinonen, Phys. Rev. B **68**, 184104 (2003).

[19]S. Hoilijoki, E. Holmstrom, and K. Nordlund, J. Appl. Phys. **110**, 043540 (2011).

[20]S. O. Kucheyev, J. S. Williams, C. Jagadish, G. Li, and S. J. Pearton, Appl. Phys. Lett. **76**, 3899 (2000).

[21]S. Kucheyev, J. Williams, and S. Pearton, Mater. Sci. Eng. R **33**, 51 (2001).

[22]T. T. Järvi, J. A. Pakarinen, A. Kuronen, and K. Nordlund, Europhys. Lett. **82**, 26002 (2008).

[23]J. F. Ziegler, J. P. Biersack, and M. D. Ziegler, SRIM: The Stopping and Range of Ions in Matter, SRIM Co., 2008.

[24]S. Plimpton, J. Comput. Phys. **117**, 1 (1995).

[25]M. Fujikane, A. Inoue, T. Yokogawa, S. Nagao, and R. Nowak, Phys. Status Solidi C **7**, 1798 (2010).

[26]Z. Wang, J. Li, F. Gao, and W. J. Weber, J. Appl. Phys. **108**, 044305 (2010).

[27]K. Nordlund, M. Ghaly, R. S. Averback, M. Caturla, T. Diaz de la Rubia, and J. Tarus, Phys. Rev. B **57**, 7556 (1998).

[28]M. Ghaly, K. Nordlund, and R. S. Averback, Philos. Mag. A **79**, 795 (1995).

[29]K. Nordlund, Comput. Mater. Sci. **3**, 448 (1995).